Electronic Supplementary Material (ESI) for Nanoscale.

Supporting Information

Polariton Waveguide Modes in Two-Dimensional Van der Waals Crystals: An Analytical Model and Correlative Nano-imaging

Fengsheng Sun,[ab†] *Wuchao Huang,*[ab†] *Zebo Zheng,*[ab†] *Ningsheng Xu,*[ab] *Yanlin Ke,*[ab] *Runze Zhan,*[ab] *Huanjun Chen,*[*ab] *and Shaozhi Deng*[*ab]

[a]State Key Laboratory of Optoelectronic Materials and Technologies, Guangdong Province Key Laboratory of Display Material and Technology, Sun Yat-sen University, Guangzhou 510275, China.

[b]School of Electronics and Information Technology, Sun Yat-sen University, Guangzhou 510006, China.

[*]Corresponding authors: chenhj8@mail.sysu.edu.cn; stsdsz@mail.sysu.edu.cn.

[†]These authors contributed equally to the work.

Note1. Solution of transverse magnetic (TM) and transverse electric (TE) waveguide modes in uniaxial and isotropic vdW crystal flake

The propagation of electromagnetic wave should satisfy the Maxwell's equations,

$$\begin{cases} \nabla \times \vec{E} = -i\omega\mu_0 \vec{H} \\ \nabla \times \vec{H} = i\omega\varepsilon_0 \overset{\leftrightarrow}{\varepsilon} \vec{E} \end{cases} \tag{S1}$$

The anisotropic permittivity tensors of the uniaxial crystal $(\varepsilon_z \neq \varepsilon_t)$ and isotropic materials $(\varepsilon_z = \varepsilon_t)$ are expressed as,

$$\overset{\leftrightarrow}{\varepsilon} = \begin{pmatrix} \varepsilon_t & 0 & 0 \\ 0 & \varepsilon_t & 0 \\ 0 & 0 & \varepsilon_z \end{pmatrix} \tag{S2}$$

A typical 2D waveguide mode with an in-plane propagation wave vector of $\vec{q}$ can be expressed as $\vec{E}(x,z,t) = \vec{e}E(z)\exp(iqx - i\omega t)$ or $\vec{H}(x,z,t) = \vec{e}H(z)\exp(iqx - i\omega t)$, where $\vec{e}$ is the unit vector of the electric field. For uniaxial and isotropic crystals, the Maxwell's equations have two independent solutions which are expressed as,

$$\begin{cases} \dfrac{\partial E_x}{\partial z} - iqE_z = -i\omega\mu_0 H_y \\ -\dfrac{\partial H_y}{\partial z} = i\omega\varepsilon_0\varepsilon_t E_x \\ iqH_y = i\omega\varepsilon_0\varepsilon_z E_z \end{cases} (TM), \quad \begin{cases} \dfrac{\partial H_x}{\partial z} - iqH_z = i\omega\varepsilon_0\varepsilon_t E_y \\ \dfrac{\partial E_y}{\partial z} = i\omega\mu_0 H_x \\ iqE_y = -i\omega\mu_0 H_z \end{cases} (TE). \tag{S3}$$

By organizing the above equation, we can obtain the expressions of the electromagnetic fields of TM and TE waves in each layer as,

$$\begin{cases} \dfrac{\partial^2 H_y}{\partial z^2} + \left(k_0^2\varepsilon_t - \dfrac{\varepsilon_t}{\varepsilon_z}q^2\right)H_y = 0, \quad (TM) \\ \dfrac{\partial^2 E_y}{\partial z^2} + \left(k_0^2\varepsilon_t - q^2\right)E_y = 0, \quad (TE) \end{cases} \tag{S4}$$

where ε_t is the in-plane dielectric constant. Parameter $k_0 = 2\pi/\lambda_0$ is the free-space wavevector. Because the waveguide modes are confined to the two interfaces, the electric and magnetic fields for the TM (E_x, H_y, E_z) modes should have the forms as,

$$H_y = \begin{cases} Ae^{-\alpha_c z}, & z \geq 0 \\ \left[A\cos(k_z z) + B\sin(k_z z)\right], & -d < z < 0 \\ \left[A\cos(k_z d) - B\sin(k_z d)\right]e^{\left[\alpha_s(z+d)\right]}, & z \leq -d \end{cases} \tag{S5}$$

$$E_x = \left(\nabla \times \overset{\vee}{H}\right)_x = \begin{cases} -\dfrac{i\alpha_c}{\omega\varepsilon_0\varepsilon_c} Ae^{-\alpha_c z}, & z \geq 0 \\ -\dfrac{ik_z}{\omega\varepsilon_0\varepsilon_t}\left[A\sin(k_z z) - B\cos(k_z z)\right], & -d < z < 0 \\ \dfrac{i\alpha_s}{\omega\varepsilon_0\varepsilon_s}\left[A\cos(k_z d) - B\sin(k_z d)\right]e^{\left[\alpha_s(z+d)\right]}, & z \leq -d \end{cases} \tag{S6}$$

$$E_z = \left(\nabla \times \overset{\vee}{H}\right)_z = \begin{cases} \dfrac{q}{\omega\varepsilon_0\varepsilon_c} Ae^{-\alpha_c z}, & z \geq 0 \\ \dfrac{q}{\omega\varepsilon_0\varepsilon_t}\left[A\sin(k_z z) - B\cos(k_z z)\right], & -d < z < 0 \\ \dfrac{q}{\omega\varepsilon_0\varepsilon_s}\left[A\cos(k_z d) - B\sin(k_z d)\right]e^{\left[\alpha_s(z+d)\right]}, & z \leq -d \end{cases} \tag{S7}$$

where $\alpha_{c,s} = \sqrt{q^2 - k_0^2\varepsilon_{c,s}}$ and $k_z = \sqrt{k_0^2\varepsilon_t - (\varepsilon_t / \varepsilon_z)q^2}$. The solutions of the (E_x, H_y, E_z) can be obtained by matching the boundary conditions at the interfaces (z = 0 and z = $-d$) as,

$$\begin{cases} E_x^{(c)} = E_x^{(w)}, & H_y^{(c)} = H_y^{(w)} \quad (z = 0) \\ E_x^{(w)} = E_x^{(s)}, & H_y^{(w)} = H_y^{(s)} \quad (z = -d) \end{cases} \tag{S8}$$

where the superscripts "c", "w", and "s" represent the cover, waveguide, and substrate layers, respectively. Consequently, the polariton modes in the waveguide and the associated dispersion relations can be obtained by solving the Equations (S1) ~ (S8). Specifically, the dispersion relation can be stated as,

$$\sqrt{\frac{\varepsilon_t}{\varepsilon_z}}\sqrt{k_0^2\varepsilon_z - q^2}\,d = \tan^{-1}\left(\frac{\sqrt{\varepsilon_t\varepsilon_z}}{\varepsilon_c}\sqrt{\frac{q^2 - k_0^2\varepsilon_c}{k_0^2\varepsilon_z - q^2}}\right) + \tan^{-1}\left(\frac{\sqrt{\varepsilon_t\varepsilon_z}}{\varepsilon_s}\sqrt{\frac{q^2 - k_0^2\varepsilon_s}{k_0^2\varepsilon_z - q^2}}\right) + m\pi \tag{S9}$$

with m = 0, 1, 2, … the orders of the TM modes.

The electric and magnetic fields of the TE (H_x, E_y, H_z) modes should have the forms as,

$$E_y = \begin{cases} Ce^{-\alpha_c z}, & z \geq 0 \\ \left[C\cos(k_z z) + D\sin(k_z z)\right], & -d < z < 0 \\ \left[C\cos(k_z d) - D\sin(k_z d)\right] e^{[\alpha_s(z+d)]}, & z \leq -d \end{cases} \tag{S10}$$

$$H_x = (\nabla \times \overset{\vee}{E})_x = \begin{cases} -\dfrac{i\alpha_c}{\omega\mu_0} Ce^{-\alpha_c z}, & z \geq 0 \\ -\dfrac{ik_z}{\omega\mu_0}\left[C\sin(k_z z) - D\cos(k_z z)\right], & -d < z < 0 \\ \dfrac{i\alpha_s}{\omega\mu_0}\left[C\cos(k_z d) - D\sin(k_z d)\right] e^{[\alpha_s(z+d)]}, & z \leq -d \end{cases} \tag{S11}$$

$$H_z = (\nabla \times \overset{\vee}{E})_z = \begin{cases} -\dfrac{q}{\omega\mu_0} Ce^{-\alpha_c z}, & z \geq 0 \\ -\dfrac{q}{\omega\mu_0}\left[C\sin(k_z z) + D\cos(k_z z)\right], & -d < z < 0 \\ -\dfrac{q}{\omega\mu_0}\left[C\cos(k_z d) - D\sin(k_z d)\right] e^{[\alpha_s(z+d)]}, & z \leq -d \end{cases} \tag{S12}$$

where $\alpha_{c,s} = \sqrt{q^2 - k_0^2\varepsilon_{c,s}}$ and $k_z = \sqrt{k_0^2\varepsilon_t - q^2}$. The solutions of the TE (H_x, E_y, H_z) modes can be obtained by matching the boundary conditions at the interfaces (z = 0 and z = –d) as,

$$\begin{cases} H_x^{(c)} = H_x^{(w)}, & E_y^{(c)} = E_y^{(w)} \quad (z = 0) \\ H_x^{(w)} = H_x^{(s)}, & E_y^{(w)} = E_y^{(s)} \quad (z = -d) \end{cases} \tag{S13}$$

Consequently, the dispersion relation of the TE modes can be stated as,

$$\sqrt{k_0^2\varepsilon_t - q^2}\, d = \tan^{-1}\left(\sqrt{\frac{q^2 - k_0^2\varepsilon_c}{k_0^2\varepsilon_t - q^2}}\right) + \tan^{-1}\left(\sqrt{\frac{q^2 - k_0^2\varepsilon_s}{k_0^2\varepsilon_t - q^2}}\right) + n\pi \tag{S14}$$

where n= 0, 1, 2, … is the orders of the TE modes.

Note 2. Calculation of isofrequency surfaces of electromagnetic waves propagating inside a homogeneous non-magnetic anisotropic crystal

The wave equation in an anisotropic crystal is,

$$\nabla^2 \vec{E} + \omega^2 \mu_0 \varepsilon_0 \overleftrightarrow{\varepsilon} \vec{E} = \nabla(\nabla \cdot \vec{E}) \tag{S15}$$

where ε_0 and μ_0 are vacuum permittivity and permeability, respectively. Equation (S15) actually contains three equations, with one for each axis. Explicitly, these equations can be expressed in the matrix form as

$$\begin{pmatrix} k_0^2\varepsilon_x - k_y^2 - k_z^2 & k_x k_y & k_x k_z \\ k_y k_x & k_0^2\varepsilon_y - k_y^2 - k_z^2 & k_y k_z \\ k_z k_x & k_z k_y & k_0^2\varepsilon_z - k_y^2 - k_z^2 \end{pmatrix} \begin{pmatrix} E_x \\ E_y \\ E_z \end{pmatrix} = 0 \tag{S16}$$

where $\vec{k}_0(k_x, k_y, k_z) = \vec{e}_k \sqrt{\omega^2 \mu_0 \varepsilon_0}$ is the wavevector of plane wave in vacuum, $\vec{e}_k$ is the unit vector of the wave vector, and $\vec{E}(E_x, E_y, E_z)$ is electric field. For non-trivial solutions of Eq. (S16), it is required that,

$$\begin{vmatrix} k_0^2\varepsilon_x - k_y^2 - k_z^2 & k_x k_y & k_x k_z \\ k_y k_x & k_0^2\varepsilon_y - k_y^2 - k_z^2 & k_y k_z \\ k_z k_x & k_z k_y & k_0^2\varepsilon_z - k_y^2 - k_z^2 \end{vmatrix} = 0 \tag{S17}$$

The isofrequency surfaces can be obtained by solving Eq. (S17) as,

$$\begin{aligned} &(\varepsilon_x k_x^2 + \varepsilon_y k_y^2 + \varepsilon_z k_z^2)(k_x^2 + k_y^2 + k_z^2) + k_0^4 \varepsilon_x \varepsilon_y \varepsilon_z \\ &- k_0^2[\varepsilon_x(\varepsilon_y + \varepsilon_z)k_x^2 + \varepsilon_y(\varepsilon_x + \varepsilon_z)k_y^2 + \varepsilon_z(\varepsilon_x + \varepsilon_y)k_z^2] = 0 \end{aligned} \tag{S18}$$

Eq. (S18) is then employed to draw the isofrequency surfaces of the biaxial α-MoO_3 crystal. In the mid-infrared region, the optical responses of the α-MoO_3 is governed by the phonon absorption, thus the permittivity of the α-MoO_3 crystal can be described using the following Lorentzian equation,[1]

$$\varepsilon_j = \varepsilon_j^\infty \left[1 + \frac{(\omega_{LO}^j)^2 - (\omega_{TO}^j)^2}{(\omega_{TO}^j)^2 - \omega^2 - i\omega\Gamma_j} \right], \quad (j = x, y, z) \tag{S19}$$

The parameter ε_j^∞ is the high frequency dielectric constant, parameters ω_{LO}^j and ω_{TO}^j are longitudinal optical (LO) and transverse optical (TO) phonon frequencies, respectively.

Parameter Γ_j is the broadening factor of the Lorentzian lineshape. The principal axes of the material are denoted by *x*, *y*, and *z*. In our study, the *x*, *y*, and *z* correspond to the crystalline directions [100], [001], and [010] of the α-MoO_3, respectively.

For uniaxial crystal $(\varepsilon_x = \varepsilon_y \neq \varepsilon_z)$, Eq. (S18) is reduced to,

$$(k_x^2 + k_y^2 + k_z^2 - k_0^2\varepsilon_x)[(k_x^2 + k_y^2)\varepsilon_x + (k_z^2 - k_0^2\varepsilon_x)\varepsilon_z] = 0 \tag{S20}$$

For isotropic crystal $(\varepsilon_x = \varepsilon_y = \varepsilon_z = \varepsilon_I)$, Eq. (S18) is further reduced to,

$$(k_x^2 + k_y^2 + k_z^2 - k_0^2\varepsilon_I)^2 = 0 \tag{S21}$$

Note 3. Calculations of the PhP interference patterns

In order to reproduce the near-field optical images in α-MoO_3 flake, we performed theoretical calculations on the PhP wave interference patterns around the circular hole. Specifically, the PhP waves were launched by the AFM tip, and the waves outside the hole were the sum of the tip-launched PhPs and those reflected from the hole edges.[2,3] Therefore, the interference wave amplitude can be expressed as,

$$\psi = \psi_0 + \sum_j \psi_j \tag{S22}$$

where ψ_0 is the tip launched PhP waves, and the waves reflected by the circular hole can be described as $\psi_j = R_j \times \psi_0 \exp\{-2\,\mathrm{Re}[\vec{q}(\theta)] \cdot \vec{r}_j(\gamma_p + i)\}$. Parameters R_j, γ_p, and $|\vec{r}_j|$ describe the reflection coefficient, PhP decay rate, and distance between the hole edge and AFM tip, respectively. The interference patterns recorded in experimental measurements are associated with $|\psi|$. To simplify the analysis, we just calculated the interference of TM_0 mode. According to the dispersion relation (Eq. (16) in the main text), the decay rate of the PhP wave can be calculated as γ_p=Im(q)/Re(q) (Fig. S3). This value should be employed in Eq. (S22) to calculate the near-field distribution. However, in the nano-imaging measurements, because the PhPs were launched into the α-MoO_3 flak from the metallic tip, due to the conversation of energy the intensity of the PhP waves will be annihilated as they are spreading away from the tip, even without any dielectric loss from the material. In addition, due to the impurities and defects introduced during fabrication of the circular hole structure (Fig. 4b in the main text), additional losses will be introduced to the PhP propagating. To take these two effects into consideration, we treated the γ_p as an adjustable parameter, whose value should be chosen to match with the experimental nano-imaging results. In a specific calculation, parameters R_j and γ_p are fixed as –1 and 0.2, respectively. A normalized amplitude $\psi_0 = 1$ is set in all of the calculations. The wave vectors $\check{q}(\theta)$ can be obtained from the in-plane dispersion relations calculated by the waveguide model. An interval of 0.5° is employed for the PhP waves propagating in all directions.

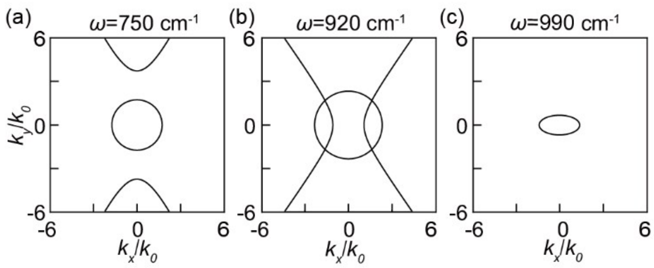

Fig. S1 In-plane isofrequency contours of the electromagnetic plane waves in the biaxial α-MoO_3 crystal. The excitation frequencies are (a) 750 cm^{-1} (Band 1), (b) 920 cm^{-1} (Band 2), and (c) 990 cm^{-1} (Band 3), respectively.

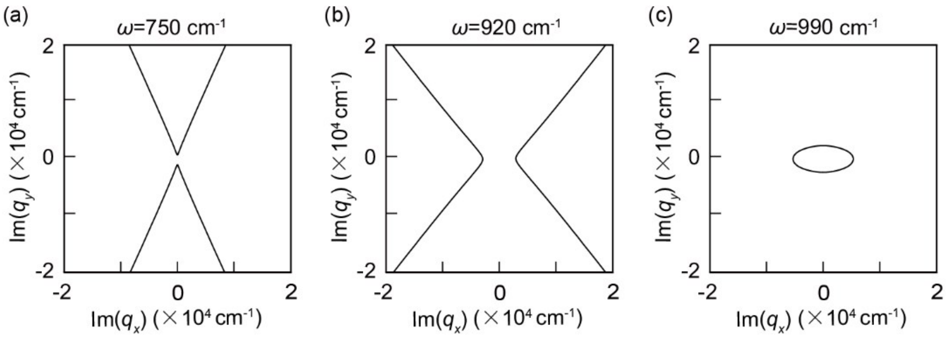

Fig. S2 In-plane contours of the imaginary part of wave vector of the PhP modes excited at 750 cm^{-1} (Band 1) (a), 920 cm^{-1} (Band 2) (b), and 990 cm^{-1} (Band 3) (c), respectively.

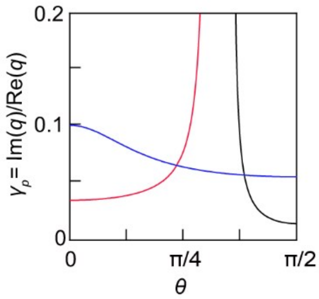

Fig. S3 Decay rates of the PhP waves propagating along different in-plane directions, which are calculated from the analytical waveguide model. The calculations are done at 750 cm^{-1} (Black line), 920 cm^{-1} (red line), and 990 cm^{-1} (blue line).

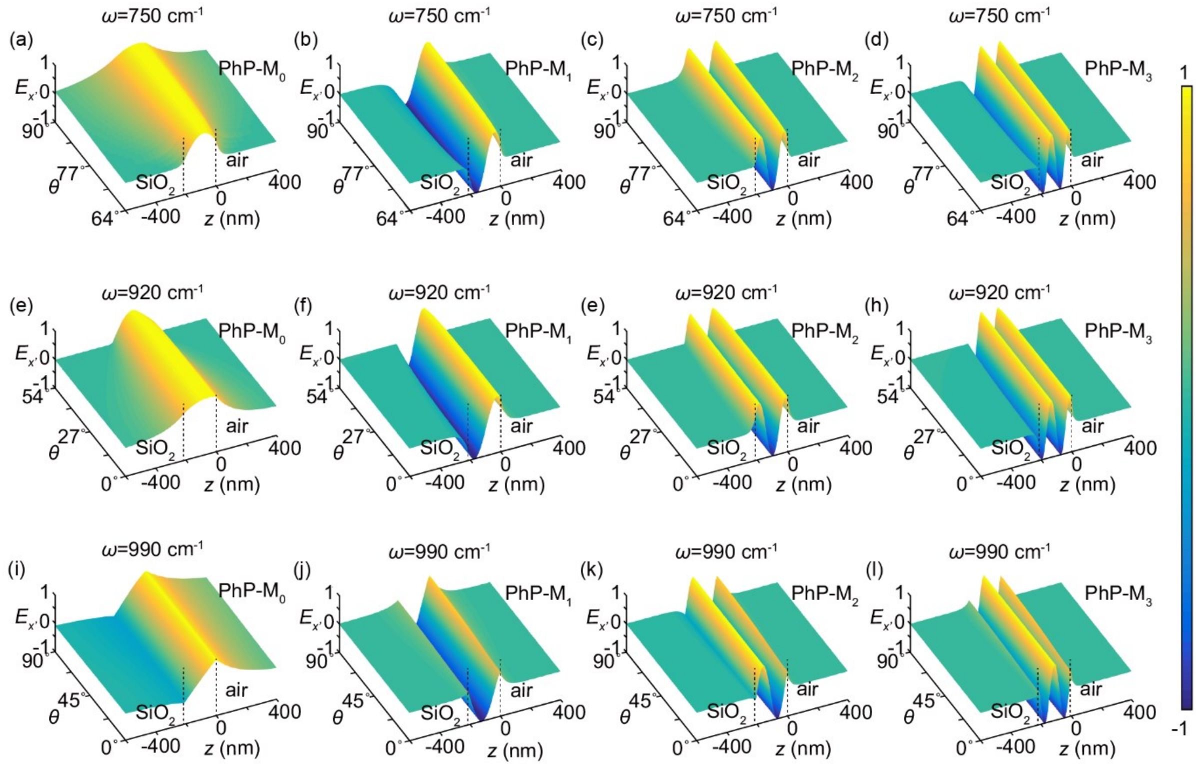

Fig. S4 Electric field E_x distributions in the 2D α-MoO_3 flake as functions of in-plane propagation angle θ. The normalized electric field amplitudes are drawn for the first four modes (l = 0, 1, 2, 3), with excitation frequencies of (a–d) 750 cm^{-1} (Band 1), (e–h) 920 cm^{-1} (Band 2), and (i–l) 990 cm^{-1} (Band 3). The thickness of the α-MoO_3 flake is 210 nm.

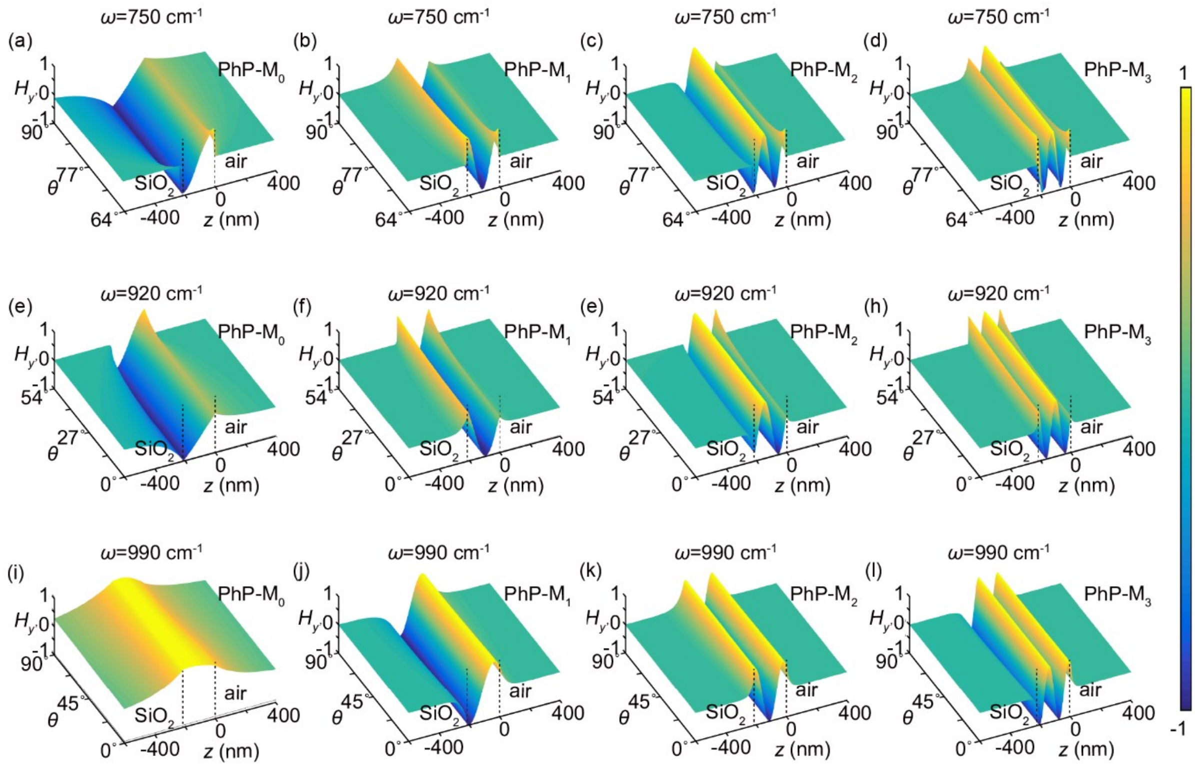

Fig. S5 Magnetic field H_y distributions in the 2D α-MoO_3 flake as functions of in-plane propagation angle θ. The normalized magnetic field amplitudes are drawn for the first four modes (l = 0, 1, 2, 3), with excitation frequencies of (a–d) 750 cm^{-1} (Band 1), (e–h) 920 cm^{-1} (Band 2), and (i–l) 990 cm^{-1} (Band 3). The thickness of the α-MoO_3 flake is 210 nm.

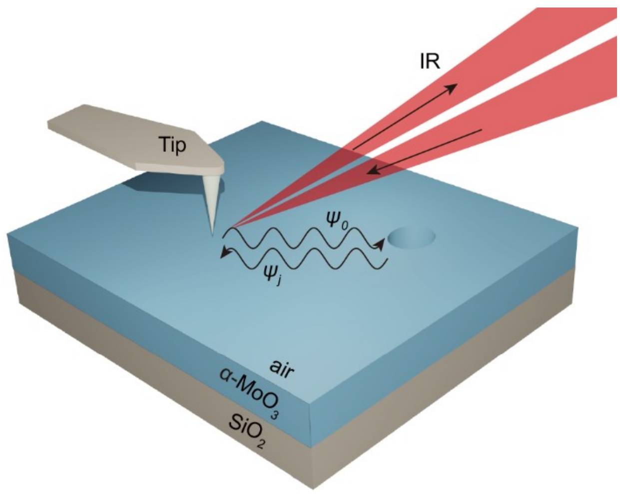

Fig. S6 Schematic showing the interference of PhP waves launched by the metallic tip with those reflected by the circular hole.

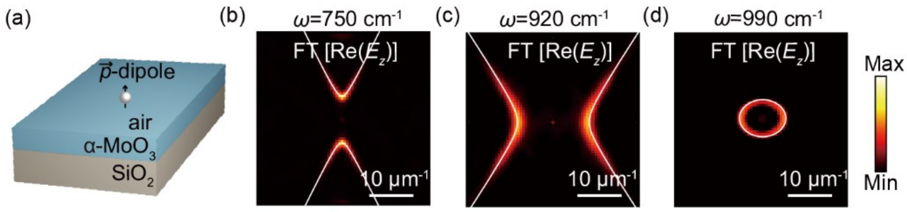

Fig. S7 FEM simulated in-plane isofrequency contours. (a) Schematic showing the FEM simulations where a vertically-polarized electric dipole source is employed to launch the PhP waves. (b–d) Fourier transformations of the 2D near-field intensities distributions calculated by the FEM simulations. The real-space of the near-field distributions are shown in Figure 4j–4l. White lines shown in (b)–(d) are results calculated by the waveguide model.

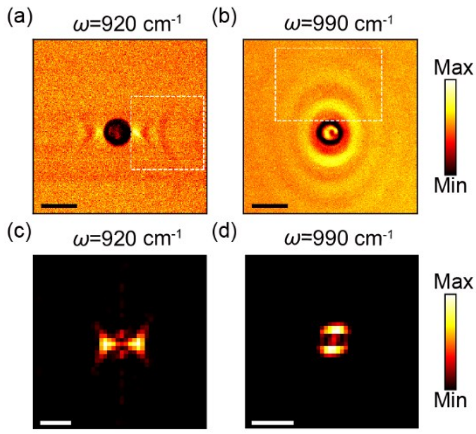

Fig. S8 (a, b) Near-filed optical intensity distributions of the α-MoO_3 flake. The excitation frequencies are (c) 920 cm^{-1} and (d) 990 cm^{-1}, respectively. Scale bars: 1 μm. (c, d) Corresponding Fourier transform images of (a) and (b). Scale bars: 20 μm^{-1}.

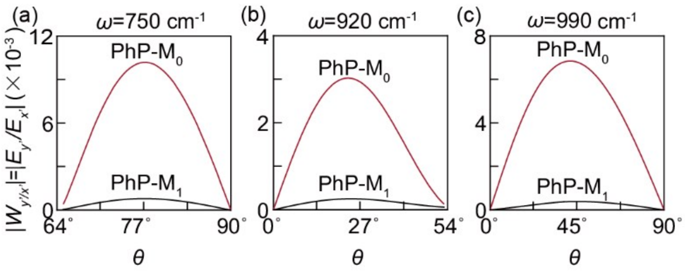

Fig. S9 Ratios between the transverse electric field amplitude ($E_{y'}$|) and longitudinal electric field amplitude (|$E_{x'}$|). The ratios are drawn for the first two PhP modes (l = 0 and 1). The excitation frequencies are 750 cm^{-1} (a), 920 cm^{-1} (b), and 990 cm^{-1} (c).

REFERENCES

(1) Zheng, Z.; Xu, N.; Oscurato, S. L.; Tamagnone, M.; Sun, F.; Jiang, Y.; Ke, Y.; Chen, J.; Huang, W.; Wilson, W. L.; Ambrosio, A.; Deng, S.; Chen. H. A mid-infrared biaxial hyperbolic van der Waals crystal. *Sci. Adv.* **2019**, *5*, eaav8690.

(2) Gerber, J. A.; Berweger, S.; O'Callahan, B. T.; Raschke, M. B. Phase-resolved surface plasmon interferometry of graphene. *Phys. Rev. Lett.* **2014**, *113*, 055502.

(3) Zheng, Z.-B.; Li, J.-T.; Ma, T.; Fang, H.-L.; Ren, W.-C.; Chen, J.; She, J.-C.; Zhang, Y.; Liu, F.; Chen, H.-J.; Deng, S.-Z.; Xu, N.-S. Tailoring of electromagnetic field localizations by two-dimensional graphene nanostructures. *Light Sci. Appl.* **2017**, *6*, e17057.